

ARTICLE

Aromatic Compounds Production from Sorbitol by Aqueous Catalytic Reforming

Jin Tan^{a,b}, Tie-jun Wang^b, Jin-xing Long^b, Qi Zhang^b, Long-long Ma^{a,b,*}, Ying Xu^b, Guan-yi Chen^a

a. School of Environmental Science and Engineering, Tianjin University, Tianjin 300072, China

b. Key Laboratory of Renewable Energy, Guangzhou Institute of Energy Conversion, Chinese Academy of Sciences, Guangzhou 510640, China

(Dated: Received on August 11, 2014; Accepted on October 20, 2014)

The rules on regulating aromatic compounds production was investigated by aqueous catalytic reforming of sorbitol. It was found that aromatics, ketones, furans, organic acids were main compounds in organic phase. The obvious effect of metal content showed that the highest carbon selectivity of aromatics was 34.36% when 3wt% Ni content was loaded on HZSM-5 zeolite modified by MCM-41. However, it was decreased only to 4.82% when Ni content was improved to 20wt%. Meanwhile, different reaction parameters also displayed important impacts on carbon selectivity. It was improved with the increase of temperature, while it was decreased as liquid hourly space velocity and hydrogen pressure was increased. The results showed that appropriate higher temperature, longer contact time and lower hydrogen pressure were in favor of aromatics information, which suggested a feasible process to solve energy crisis.

Key words: Aromatic compound, Sorbitol, Aqueous catalytic reforming, Composite catalyst

I. INTRODUCTION

Energy crisis has become a serious problem for all the countries in the world. Recently, much more attention has been focused on the gasoline component additives which are mainly composed of benzene, toluene and xylenes [1, 2]. However, these aromatic compounds are usually derived from the sharply depleting fossil fuel. Therefore, it is urgent to exploit a new route for producing aromatic compounds from renewable biomass to substitute those originated from fossil fuels.

Usually, substantial efforts have been concentrated on three main technical routes: (i) biomass pyrolysis, especially catalytic fast pyrolysis (CFP), under high temperature above 873 K [3–7]. Although aromatic compounds could be produced from biomass over bifunctional catalysts directly, a large amount of coke would be inevitably formed during the pyrolysis process, resulting in the durative deactivation of catalysts [5]. (ii) Gasification synthesis [8]. Carbon oxide and hydrogen are main components of synthesis gas, and then aromatic products are synthesized by Fischer-Tropsch synthesis. However, there are no aromatic products during Fischer-Tropsch synthesis at low temperature and the yield of aromatic compounds are about only 6%

even at high temperature [9]. Moreover, coke is also main byproduct. (iii) Aqueous phase catalytic reforming [10, 11]. Converting biomass into aromatic compounds by aqueous phase catalytic reforming has attracted more and more attentions due to its two obvious advantages. It is easy to obtain final rough aromatic products distributed in organic phase, which will be separated from aqueous phase automatically. Furthermore, lower energy consumption is the second superiority of aqueous phase catalytic reforming compared with pyrolysis and gasification synthesis. Many kinds of platform chemicals have been selected as feedstock to produce aromatic compounds through aqueous phase catalysis, for example glycerol could be converted into alkyl-aromatic over HZSM-5 combined with Pd/ZnO at 673 K under 2 MPa hydrogen pressures [7]. Furan compounds were also chosen as raw material to investigate the aromatic formative mechanism only using HZSM-5 zeolite at different temperature ranges [4]. High concentration of sorbitol (60wt%) was converted into hydrophobic substances firstly over Pt-Re/C catalyst, and then aromatics was produced through ZSM-5 zeolite [12].

Although a great deal of effort has been made on the aromatic formation by aqueous phase catalytic reforming, different kinds of precious metal are usually adopted to achieve better results. Moreover, undesired coke also inevitably appeared during reaction under harsh conditions. These would cause much difficulty in the application for industrialization. But adding meso-

* Author to whom correspondence should be addressed. E-mail: mall@ms.giec.ac.cn, Tel.: +86-20-87048614, FAX: +86-20-87057751

pores into HZSM-5 catalyst was able to overcome diffusion limitation and char formation [13]. Furthermore, in our previous investigation, the Ni/HZSM-5 catalyst modified by MCM-41 showed exciting performance on the C5-C6 alkanes production from sorbitol [14]. Therefore, in this work, cheaper metal Ni and composite zeolites were adopted in this reaction. The effect of reaction parameters such as reaction temperature, LHSV (liquid hourly space velocity), GHSV (gas hourly space velocity), hydrogen pressure as well as different metal content on composite zeolites were investigated in detail to illustrate the rule of aromatic compounds production.

II. MATERIALS AND METHODS

A. Materials

Sorbitol (analytical reagent) was purchased from Aladdin reagent company, Shanghai, China. HZSM-5 and MCM-41 were purchased from catalyst plant of Naikai University. Nickel nitrate (analytical reagent) was bought from Fuchen chemical reagents factory, Tianjin, China.

B. Catalyst preparation

The composite catalysts used in this work were synthesized by an incipient wetness impregnation method. Nickel nitrate solution and composite zeolites (HZSM-5:MCM-41 weight ratio was 3:2) were mixed together. This mixture was then dried overnight at 393 K and calcinated at 773 K for 4 h in air. After cooling down to room temperature, catalyst powders were compressed by a bead machine and selected by 40–60 mesh sieves. The Ni content of catalysts ranged from 1% to 20%, respectively.

C. Catalyst characterization

The crystalline structure of catalysts were characterized by X-ray diffraction (XRD) (X Pert Pro MPD with Cu K α ($\lambda=0.154$ nm) radiation, Philip) operated at 40 kV and 100 mA. Scanning angle (2θ) ranged from 5° to 80°.

Brunauer-Emmett-Teller (BET) surface area, external surface area, pore volume of catalysts were determined by nitrogen adsorption at 77 K using a QUADRASORB SI analyzer equipped with QuadraWin software system. All samples were degassed at 573 K for 8 h before adsorption measurement. After measurement, surface areas were calculated by the BET method and mesoporous pore volumes were calculated with the Barret-Joyner-Halenda (BJH) model. Micropore volumes were calculated with the T-plot method.

D. Experimental setups and procedures

Catalytic performance was conducted in a stainless-steel tubular flow reactor. Hydrogen gas moved in a down flow direction with sorbitol solution, and both of them were heated by an electric heating furnace. The catalysts of 4.0 g were filled in reactor and silica wools were also filled at the both ends of catalysts. Prior to catalytic performances test, catalysts were reduced *in situ* by a flow of H₂ (30 mL/min) at 773 K for 4 h and then cooled down to reaction temperature. After that, H₂ pressure, LHSV, and GHSV were adjusted to the designed conditions and then sorbitol solution was pumped into tubular to start reaction after being preheated at a certain temperature. Liquid products were accumulated in a gas-liquid separator and drained periodically into a collecting container. The analysis of oil products was performed on an Agilent GC-7890A gas chromatograph (HP innowax capillary column 19091N-133N, 30 m \times 250 μ m \times 0.25 μ m) equipped with a mass spectrometer (5975C) using 99.995% of He as carrier gas. The conversion of feedstock was detected by HPLC (Waters 2695). Total organic carbon in aqueous phase was tested by TOC (Elementar in German Vario TOC). Sorbitol conversion X and carbon selectivity S of aqueous phase were calculated according to the following equations:

$$X = \frac{x_{in} - x_{out}}{x_{in}} \times 100\% \quad (1)$$

$$S = \frac{x_{total}}{x_{in}} \times 100\% \quad (2)$$

where x_{in} , x_{out} , and x_{total} are sorbitol in, sorbitol out, and total carbon aqueous.

III. RESULTS AND DISCUSSION

A. XRD characterization of catalysts

XRD patterns of composite catalysts with different Ni loadings are shown in Fig.1. XRD characteristic peaks at 2θ of 37.5°, 43.4°, and 63.2° were found over the catalysts, which can be attributed to the [111], [200], and [220] crystal faces of nickel oxide, respectively. Meanwhile, the peak intensity was increased sharply as Ni content was improved gradually, and it showed the highest peak intensity of catalyst when the Ni loading was increased to 20wt%. It indicated that inculcating crystals were easy to gather and form more regular nickel oxide crystals absorbed on the surface of composite zeolites.

B. BET characterization

Table I lists the physicochemical properties of the composite catalysts before reaction. The BET surface area of pure composite zeolites was found to be

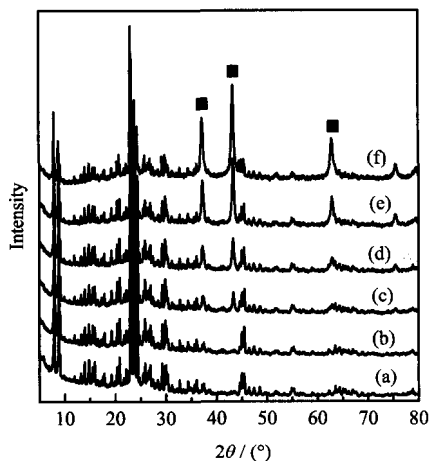


FIG. 1 XRD patterns of different Ni content on composite zeolites. (a) 0wt%Ni, (b) 1wt%Ni, (c) 3wt%Ni, (d) 5wt%Ni, (e) 10wt% Ni, and (f) 20wt%Ni.

TABLE I Physicochemical properties of composite catalysts before reaction including surface area A in m^2/g and volume V in mL/g .

Catalyst*	A_{BET}	A_{ext}	V_{mic}	V_{mes}
H+M	527.52	360.63	0.18	0.38
1wt%Ni/H+M	470.97	316.37	0.16	0.53
3wt%Ni/H+M	497.45	364.48	0.16	0.41
5wt%Ni/H+M	457.17	457.17	0.15	0.64
10wt%Ni/H+M	398.30	284.02	0.13	0.51
20wt%Ni/H+M	318.02	316.03	0.10	0.87

* H: HZSM-5, M: MCM-41.

$527.52 \text{ m}^2/\text{g}$. When Ni component was loaded, the surface area of composite catalysts was decreased, and it was decreased to $318.02 \text{ m}^2/\text{g}$ when Ni content was up to 20wt%. The average pore diameter data (Fig.2) showed that composite catalysts had two typical pore structures (micropore and mesoporous). Nevertheless, the average mesoporous diameter was decreased obviously after different Ni content was loaded, which resulted in the new formative pores by metal filling action. This result showed that the influence of metal content on mesoporous diameter was much greater than that of micropore.

C. The effect of different parameters on aromatics variation

1. The effect of Ni content

The effect of Ni content on oil components distribution was conducted in the range of 1wt%–20wt%. Sorbitol conversion and total carbon selectivity in aqueous phase are shown in Fig.3. It could be clearly seen from

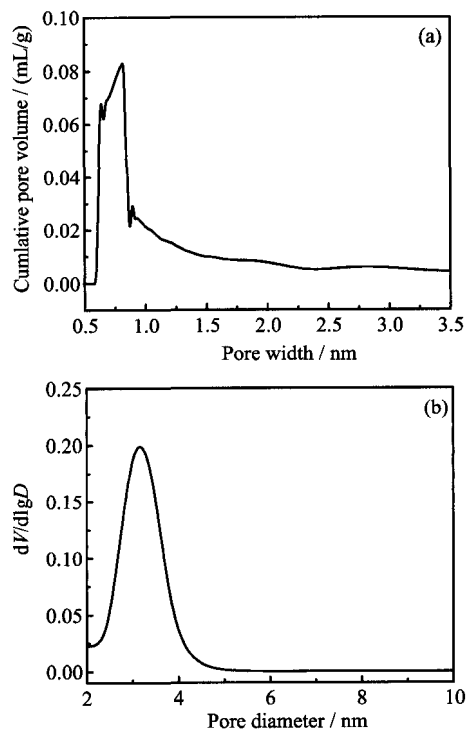


FIG. 2 Pore diameter distribution of composite catalysts. (a) Micropore and (b) mesoporous.

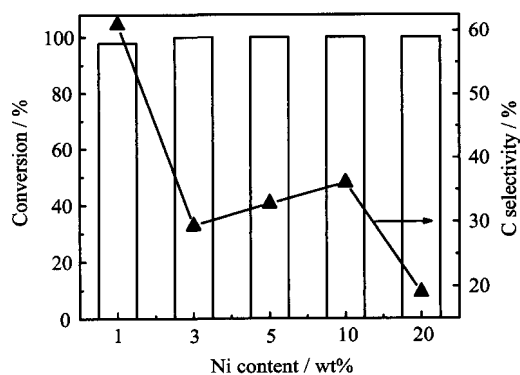


FIG. 3 Sorbitol conversion and carbon selectivity in aqueous phase after aqueous catalysis reforming. Reaction conditions: H_2 pressure=4.0 MPa, $T=553 \text{ K}$, LHSV=1.5 h^{-1} , GHSV=1000 h^{-1} , and sorbitol: 20 wt%.

Fig.3 that sorbitol conversion nearly reached a maximum value of 100% over different Ni content catalysts. However, the total carbon selectivity in aqueous was 60.99% when Ni content was 1wt%. This result indicated that oxygen species in sorbitol molecules could not be fully removed under such reaction conditions. Majority products were hydrophilic existing in aqueous phase. But the carbon selectivity was the lowest and only reached 20.23% when 20wt%Ni content catalyst was used, implying that more Ni content absorbed on the zeolites was in favor of hydrodeoxygenation reaction to form hydrophobic compounds. In fact, those

TABLE II Carbon selectivity of different oil components after reaction over various catalysts.

Catalysts*	Carbon selectivity/%				
	Aromatic	Ketone	Furan	Org. acid	Others
3wt%Ni/H+M	34.36	13.85	14.30	Trace	6.92
5wt%Ni/H+M	15.34	26.29	9.77	0.43	6.54
10wt%Ni/H+M	18.05	24.75	8.32	Trace	7.73
20wt%Ni/H+M	4.82	49.19	4.70	Trace	4.83

* H: HZSM-5, M: MCM-41.

hydrophilic chemicals, like propanal, acid, ester, ketone [13], glycerol [7] and furans [4], could yield aromatics at different selectivity. It revealed that hydrophilic compounds were intermediate chemicals when sorbitol was catalyzed into aromatics.

Table II lists the carbon selectivity of main components in oil phase. The result of catalysis over 1%Ni content catalyst was not shown here due to poor oil yield, which was unable to be analyzed. The highest carbon selectivity of aromatics was 34.36% when 3wt%Ni content catalyst was used. But it was decreased to 4.82% when Ni content was up to 20wt%. Obviously, 3wt%Ni content catalyst showed a wonderful performance on aromatics production. The synergic action between metal and composite zeolites could play a vital role in the aromatization. Higher metal content catalyst would lead to bonds cracking easily, resulting in low carbon compounds formation. Therefore, we chose 3wt%Ni content as optimum load and investigated the regulation of temperature, LHSV, GHSV and hydrogen pressure on aromatics production next.

2. The effect of temperature

The effect of reaction temperature on aromatics production was conducted at the range of 513 K to 593 K. As shown in Fig.4, the activity of catalyst showed lower performance at 513 K, and sorbitol conversion was 77.38%. Although sorbitol conversion reached a maximal value of 100% at 533 K, there was nearly no oil appearing in final liquid phase, which was homogeneous. 78.31% and 65.96% carbon derived from feedstock was found in the aqueous phase at 513 and 533 K, respectively. This result suggested that lower temperature was not in favor of hydrodeoxygenation reaction. Majority C–O bonds were main structure of aqueous compounds. However, the carbon selectivity of aqueous phase was decreased to 13.46% as temperature was improved to 593 K. Meanwhile, the carbon selectivity of aromatics was increased from 27.28% to 41.86% (Table III). These results implied that hydrodeoxygenation and aromatization reactions were easier to occur at higher temperatures. But coke formation was inevitable over catalysts under harsh conditions, indicating the crack-

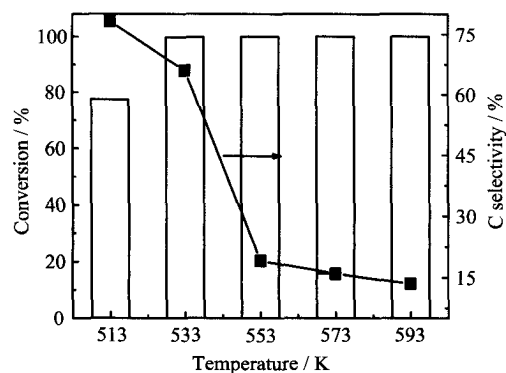


FIG. 4 Sorbitol conversion and carbon selectivity in aqueous phase under different temperature. Reaction conditions: H_2 pressure=4.0 MPa, LHSV=1.5 h^{-1} , GHSV=500 h^{-1} , sorbitol=20%.

TABLE III Effect of temperature on carbon selectivity of oil components.

T/K	Carbon selectivity/%				
	Aromatic	Ketone	Furan	Organic acid	Others
553	27.28	8.35	4.11	6.16	33.19
573	28.22	19.93	4.14	7.36	20.09
593	41.86	20.42	7.32	5.59	6.01

ing of sorbitol by pyrolysis [10, 15]. Furthermore, C–C bonds cleavage activity was strengthened under high temperature over metal catalyst, resulting in light hydrocarbon production [16].

3. The effect of LHSV

Various LHSV conditions were adopted to investigate the effect of residence time of feedstock with catalyst to aromatics production. As shown in Fig.5, sorbitol conversion always kept a maximal value of 100% when LHSV was at the range of 0.75 h^{-1} to 3.00 h^{-1} . But it was decreased to 29.77% sharply at 6.00 h^{-1} . The change of carbon selectivity in aqueous phase was correspondent with that of LHSV. Carbon selectivity was increased from 1.62% to 74.94% obviously when LHSV was improved from 0.75 h^{-1} to 6.00 h^{-1} . These results indicated that perfect conversion could be achieved at longer contact time of feedstock with catalyst. Meanwhile, the carbons in feedstock could be better shifted from aqueous phase to oil phase. The results in Table IV further showed that residence time was a key factor not only in hydrodeoxygenation reaction, but also in aromatization reactions. For example, the carbon selectivity of aromatics reached the highest value of 65.65% when LHSV was at 0.75 h^{-1} . But it was decreased to 9.34% drastically when LHSV was only reduced to 2.25 h^{-1} . Although sorbitol was nearly converted com-

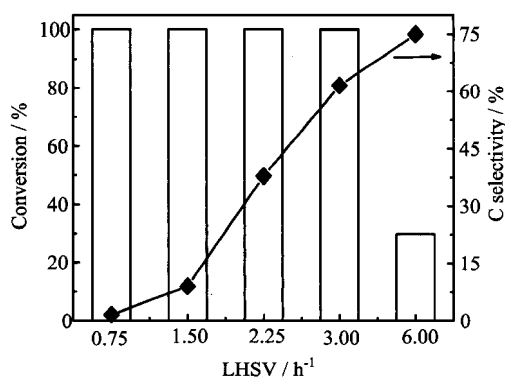


FIG. 5 Effect of LHSV on sorbitol conversion and carbon selectivity in aqueous phase. Reaction conditions: H_2 pressure=4.0 MPa, $T=553$ K, GHSV=50 h^{-1} , sorbitol=20%.

TABLE IV Effect of LHSV on carbon selectivity of oil products. LHSV in h^{-1} .

LHSV	Carbon selectivity/%				
	Aromatic	Ketone	Furan	Organic acid	Others
0.75	65.65	Trace	Trace	4.65	25.47
1.50	30.90	9.46	4.66	6.98	37.59
2.25	9.34	13.38	3.30	8.81	14.84

pletely when LHSV was at 3.0 h^{-1} , the final products formed a homogeneous aqueous solution, let alone aromatics production. These hydrophilic substances need to be further reacted to remove oxygen atoms from self-structure to form aromatics and other hydrophobic compounds by dehydrogenation, decarbonylation and aromatization reactions [10, 17, 18].

4. The effect of GHSV

Figure 6 shows the effect of GHSV on sorbitol conversion and aqueous carbon selectivity. There was little change on sorbitol conversion under various GHSV ranging from 500 h^{-1} to 4000 h^{-1} , and reached the maximum value of 100%. However, carbon selectivity in aqueous was increased from 17.96% to 35.89% as GHSV was improved from 500 h^{-1} to 4000 h^{-1} . These results indicated that GHSV of hydrogen also played a vital role in hydrodeoxygenation reaction as Ni content, temperature and LHSV. In fact, sorbitol could be first converted into hydrophilic substances over Ni catalysts without hydrogen. And then, these intermediate compounds were further converted into aromatics and hydrocarbon compounds in the presence of hydrogen and catalysts simultaneously. Majority of intermediate compounds could not be further converted completely when hydrogen flew fast through catalyst mixed with feedstock. There was no enough time for hydrogen to adsorb on the metal surface to engage in hydrodeoxy-

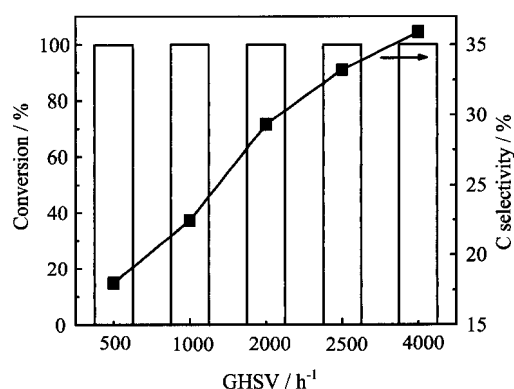


FIG. 6 Effect of GHSV to sorbitol conversion and carbon selectivity in aqueous phase. Reaction conditions: H_2 pressure=4.0 MPa, $T=553$ K, LHSV=2.25 h^{-1} , sorbitol=20%.

TABLE V Effect of GHSV on carbon selectivity of oil products. GHSV in h^{-1} .

GHSV	Carbon selectivity/%				
	Aromatic	Ketone	Furan	Organic acid	Others
500	14.97	21.45	5.30	14.12	23.79
1000	16.30	20.64	2.26	13.80	14.59
2000	11.73	18.84	2.19	11.07	22.27
2500	6.07	18.43	0.40	11.25	26.77
4000	3.40	17.43	3.78	8.79	29.12

genation and aromatization reactions. Our investigation results shown in Table V confirmed this opinion, which was in accordance with that of olazar [19]. It was obviously found that the carbon selectivity of aromatics was at the lowest value of 3.40% when GHSV was at 4000 h^{-1} .

5. The effect of hydrogen pressure

The results of hydrogen pressure effect on catalytic performance are listed in Fig.7. Sorbitol conversion reached a perfect value of 100% under various hydrogen pressures. However, carbon selectivity in aqueous was increased from 17.77% to 42.39% when hydrogen pressure was improved from 1.0 MPa to 5.0 MPa. This result indicated that majority carbon remained in hydrophilic compounds, and higher pressure could cause inhibition to hydrodeoxygenation and aromatization reactions. Hydrogen pressure could be used to adjust the relative rates of C-C versus C-O bond cleavage. Improving system pressure increased the hydrogen concentration and most likely resulted in a decrease in the rate of dehydrogenation [17, 21].

The results in Table VI were in accordance with this opinion. Carbon selectivity of aromatics was decreased from 46.02% to 4.48% when hydrogen pressure was im-

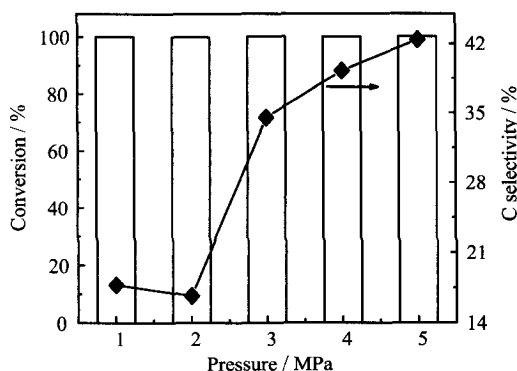


FIG. 7 Sorbitol conversion and carbon selectivity in aqueous phase varied with hydrogen pressure. Reaction conditions: $T=553$ K, $LHSV=2.25$ h^{-1} , $GHSV=2500$ h^{-1} , sorbitol=20%.

TABLE VI Effect of hydrogen pressure on carbon selectivity of oil products.

P/MPa	Carbon selectivity/%				
	Aromatic	Ketone	Furan	Organic Acid	Others
1.0	46.02	11.22	0.93	7.48	10.63
2.0	36.88	19.13	1.79	10.25	9.93
3.0	14.05	16.01	1.49	9.72	16.82
4.0	5.37	16.28	0.35	9.94	23.65
5.0	4.48	17.74	1.98	8.09	20.15

proved from 1.0 MPa to 5.0 MPa. The dehydrogenation was inhibited heavily at higher hydrogen pressure, resulting in the decrease of aromatics.

IV. CONCLUSION

The regulation of aromatic compounds production were proposed through aqueous catalytic reforming of sorbitol. Results showed that the highest carbon selectivity of aromatics was 34.36% over 3wt%Ni loading dosage catalyst. Meanwhile, higher temperature, longer contact time and lower pressure are in favor of aromatics formation. The optimized result of aromatic compounds can be obtained at 593 K, 1.0 MPa H_2 , and 0.75 h^{-1} of LHSV. Therefore, the results presented in this work suggest a strategy for developing a feasible process to produce aromatic compounds for sorbitol derived from biomass.

V. ACKNOWLEDGMENTS

This work was supported by the National Key Basic Research and Development Plan (No.2012CB215304), the Key Laboratory of Renewable Energy Foundation (No.y407j51001), the National Natural Science Foundation of China (No.51376185 and No.51106108), the National High-Tech Research and Development Programme (No.2012AA101806).

- [1] T. R. Carlson, G. A. Tompsett, W. C. Conner, and G. W. Huber, *Top. Catal.* **52**, 241 (2003).
- [2] Y. T. Cheng, J. Jae, J. Shi, W. Fan, and G. W. Huber, *Angew. Chem. Int. Edit.* **51**, 1387 (2012).
- [3] K. Y. Chen, M. Tamura, Z. Yuan, Y. Nakagawa, and K. Tomishige, *ChemSusChem* **6**, 613 (2013).
- [4] Y. T. Cheng and G. W. Huber, *ACS Catal.* **1**, 611 (2011).
- [5] J. W. Diehl and F. P. Di Sanzo, *J. Chromatogr. A* **1080**, 157 (2005).
- [6] R. A. Dagle, J. A. Lizarazo-Adarme, V. L. Dagle, M. J. Gray, J. F. White, D. L. King, and D. R. Palo, *Fuel Process. Technol.* **123**, 65 (2014).
- [7] T. Q. Hoang, X. L. Zhu, T. Danuthai, L. L. Lobban, D. E. Resasco, and R. G. Mallinson, *Energ. Fuel.* **24**, 3804 (2010).
- [8] S. Ilias and A. Bhan, *J. Catal.* **311**, 6 (2014).
- [9] T. Juganaru, C. Ionescu, D. Bombos, M. Bombos, and V. Matei, *Rev. Chim.* **58**, 698 (2007).
- [10] J. Jae, R. Coolman, T. J. Mountziaris, and G. W. Huber, *Chem. Eng. Sci.* **108**, 33 (2014).
- [11] J. Jae, G. A. Tompsett, A. J. Foster, K. D. Hammond, S. M. Auerbach, R. F. Lobo, and G. W. Huber, *J. Catal.* **279**, 257 (2011).
- [12] E. L. Kunkes, D. A. Simonetti, R. M. West, J. C. Serrano-Ruiz, C. A. Gärtner, and J. A. Dumesic, *Science* **17**, 417 (2008).
- [13] X. L. Zhu, L. L. Lobban, R. G. Mallinson, and D. E. Resasco, *J. Catal.* **271**, 88 (2010).
- [14] Q. Zhang, T. Jiang, B. Li, T. J. Wang, X. H. Zhang, Q. Zhang, and L. L. Ma, *ChemCatChem* **4**, 1084 (2012).
- [15] T. R. Carlson, J. Jae, Y. C. Lin, G. A. Tompsett, and G. W. Huber, *J. Catal.* **270**, 110 (2010).
- [16] L. Vilcocq, A. Cabiacc, C. Especel, S. Lacombe, and D. Duprez, *Catal. Today* **189**, 117 (2012).
- [17] N. Li and G. W. Huber, *J. Catal.* **270**, 48 (2010).
- [18] C. A. Mullen, A. A. Boateng, D. J. Mihalcik, and N. M. Goldberg, *Energ. Fuel* **25**, 5444 (2011).
- [19] M. Olazar, R. Aguado, J. Bilbao, and A. Barona, *Aiche J.* **46**, 1025 (2000).
- [20] B. M. Moreno, N. Li, J. Lee, G. W. Huber, and M. T. Klein, *RSC Adv.* **3**, 23769 (2013).

层结点, 分别采用4:21:1、4:24:1、4:24:1的网络结构, 利用BP算法获得了三个令人满意的QSPR模型, 其总相关系数R分别为0.9999、0.9997和0.9995, 标准误差分别为1.036、1.469和1.510, 利用该模型得到的 S° 、 $\Delta_f H^{\circ}$ 和 $\Delta_f G^{\circ}$ 的预测值, 与文献值的相对平均误差分别为0.11%、0.34%和0.24%, 两者吻合度非常理想, 说明该模型具有很好的稳定性、相关度和预测能力, 结果表明多溴代二苯胺的热力学性质与 0X 、 K_{31} 、 M_{29} 和 M_{36} 有很好的非线性关系, 证明利用新定义的取代基指数建立的ANN模型对多溴代二苯胺性质的预测是合理的、适用的。

关键词: 多溴代二苯胺, 神经网络, 分子形状指数, 电性距离矢量, 取代基指数, 热力学性质

碳化物形成对石墨烯生长的影响 65

王淮准, 罗其全, 张文华, 李震宇* (中国科学技术大学合肥微尺度国家实验室, 合肥 230026)

摘要: 选取了一个典型的金属碳化物体系 Mo_2C 对其形成在石墨烯生长中的作用进行了基于第一性原理的理论研究。碳在 Mo_2C 体相中扩散十分困难, 而在 $Mo_2C(001)$ 表面则变得比较容易。因此抑制碳析出和表面石墨烯生长可以同时实现。在 $Mo_2C(101)$ 表面碳扩散的难易程度依赖于扩散方向。相对于(001)表面, (101)表面不利于石墨烯生长。

关键词: 碳化钼, 扩散, 密度泛函理论

高稳定电化学扫描隧道显微镜研制 70

夏志刚^{a,b}, 王纪浩^{a,b}, 侯玉斌^a, 陆轻轴^{a,b*} (a. 中国科学院强磁场科学中心和中国科学技术大学, 合肥 230026; b. 中国科学技术大学合肥微尺度物质科学国家实验室(筹), 合肥 230026)

摘要: 展示了一台自制的电化学扫描隧道显微镜。这台电化学STM具有很高的稳定性, 它在XY平面和Z方向的漂移速率分别为每分钟67和55.6 pm/min。另外, 特殊设计的扫描管部件有效地避免了在高湿度的环境中大漏电流的产生。详细描述了这台电化学STM的机械结构。通过在硫酸铜溶液中测量STM图像证明这套系统的优异性能, 得到了大范围干净有序的Au(111)表面和高分辨的高聚石墨原子图像。

关键词: 扫描隧道显微镜, 电化学, 高稳定

$Tm^{3+}/Yb^{3+}:LiYF_4$ 单晶的高效近红外量子剪裁及其在光伏电池中的应用 73

符立^a, 夏海平^{a*}, 董艳明^a, 李珊珊^a, 谷雪梅^a, 章践立^a, 王冬杰^a, 江浩川^b, 陈宝玖^c (a. 宁波大学光电功能材料重点实验室, 宁波 315211; b. 中国科学院宁波材料与技术工程研究所, 宁波 315211; c. 大连海事大学物理系, 大连 116026)

摘要: 采用改进的坍塌下降法成功地生长了 Tm/Yb 共掺氟化钇锂单晶。该单晶体具有每吸收一个蓝色光子并能发射出2个1000 nm近红外光子的下转换发光效应。测定了样品的激发光谱、发射光谱和荧光衰减曲线。在465 nm蓝光激发下观察到由 $Yb^{3+}: ^2F_{5/2} \rightarrow ^2F_{7/2}$ 能级跃迁所致的960~1050 nm波段的发射带, 此发光带源于 Tm^{3+} 对 Yb^{3+} 离子的能量下转换过程。应用Inokuti-Hirayama模型, 研究了晶体的能量转换过程, 结果表明 Tm^{3+} 向 Yb^{3+} 的能量传递是一个电偶极子相互作用机制过程。当 Tm^{3+} 与 Yb^{3+} 离子的掺杂浓度为0.49mol%与5.99mol%时, 单晶的量子剪裁效率达到最大值167.5%。

关键词: 量子剪裁, 能量传递, $LiYF_4$ 单晶, Tm^{3+}/Yb^{3+}

铋纳米线中电导的温度依赖性 79

霍鹏程, 费广涛*, 张阳, 张立德 (中国科学院合肥物质科学研究院固体物理研究所, 中国科学院材料物理重点实验室, 安徽省纳米材料与纳米技术重点实验室, 合肥 230031)

摘要: 采用电沉积的方法在多孔氧化铝模板中合成了直径为30 nm且沿着[0112]方向生长的单晶铋纳米线, 测量了纳米线电导随着温度78~320 K变化的关系曲线。结果发现, 其半导体转变的温度为230 K, 且纳米线的电导有很强的温度依赖性。

关键词: 铋纳米线, 半导体转变, 电导

分级多孔 $CaFe_2O_4/C$ 的合成及其微波催化活性 84

宋艺, 孔超, 李嘉* (济南大学材料科学与工程学院, 济南 250022)

摘要: 以天然木棉为模板, 利用造孔及纳米颗粒自组装两步法合成了分级多孔的 $CaFe_2O_4/C$ 复合催化剂。 $CaFe_2O_4/C$ 复合催化剂保留了木棉模板的中空纤维形貌, 且该中空纤维是由碳及均匀分布在碳表面的 $CaFe_2O_4$ 纳米颗粒组成。该复合催化剂具有较强的甲基紫微波催化降解活性。研究了 $CaFe_2O_4$ 负载量、微波功率、催化剂用量、甲基紫的初始浓度和pH值对微波诱导甲基紫降解的影响。结果表

明, $CaFe_2O_4/C$ 微波降解甲基紫的催化反应具有较高的反应速率和较短的反应时间。其降解反应符合一级动力学模型。 $CaFe_2O_4/C$ 高的催化活性得益于催化反应和吸附特性之间的协同作用。

关键词: 铁酸钙, 微波, 催化活性, 木棉, 降解

三芳胺和二氢吡啶作为给体的染料对钴电解质的染料敏化太阳能电池性能的影响 91

张月^a, 王志辉^b, 郝玉杰^b, 武全萍^a, 梁茂^b, 薛松^{b*} (a. 天津理工大学自动化学院控制理论与应用天津市重点实验室, 天津 300384; b. 天津理工大学化学化工学院, 天津 300384)

摘要: 合成了两种有机染料, 三芳胺染料 $XS51$ 和二氢吡啶染料 $XS52$, 并分别用于钴基电解质和碘基电解质的染料敏化太阳能电池中。考察了染料结构对光物理性能、电化学性能和电池性能的影响。 $XS51$ 为含有四个己氧基的三芳胺结构, 表现出较好的空间位阻, 从而提高了光电电压。 $XS52$ 中二氢吡啶的给电子能力强, 从而短路电流较大。同碘电解质相比, 所合成的染料更适合用于钴电解质的染料敏化电池中。在100 mW/cm²的光强下, 基于染料 $XS52$ 的钴电解质太阳能电池总的光电转换效率达到6.58%。

关键词: 染料敏化太阳能电池, 二氢吡啶, 三芳胺, 光伏性能, 钴电解质

山梨醇水相催化重整制芳香化合物 101

谈金^{a,b}, 王铁军^b, 龙金星^b, 张琦^b, 马隆龙^{a,b*}, 陈冠益^a (a. 天津大学环境科学与工程学院, 天津 300072; b. 中国科学院广州能源研究所可再生能源重点实验室, 广州 510640)

摘要: 研究了山梨醇水相催化重整对制备芳烃类化合物的调控规律。研究表明, 芳烃类、酮类、呋喃类及有机酸类化合物为油相的主要成分。当3%的镍负载在复合分子筛时, 芳烃碳收率达到了34.36%; 而当金属负载量达到20%时, 碳收率仅为4.82%。同时, 不同的反应参数对碳收率也有较大的影响。碳收率随着温度的升高逐渐增大; 但随着液时空速与氢气压力的增加而减小。因此, 合适的温度、较长的滞留时间及较低的气压压力有利于芳烃的生成。

关键词: 芳香化合物, 山梨醇, 水相催化重整, 复合催化剂

辐射接枝法制备膨化聚四氟乙烯杂化膜及其抗菌性表征 107

王运龙^a, 汪谟贞^{a*}, 吴启超^b, 周晓^b, 葛学武^a (a. 中国科学院物质化学重点实验室, 中国科学技术大学高分子材料科学与工程系, 合肥 230026; b. 广东天安新材料股份有限公司, 佛山 528000)

摘要: 通过共辐射接枝的方法, 将聚丙烯酸成功接枝到膨化聚四氟乙烯薄膜上。采用 $NaBH_4$ 还原吸附在接枝链上的银离子, 在膜中原位负载银纳米粒子, 制备了抗菌性ePTFE杂化膜。杂化膜的SEM、XPS、XRD和TGA表征结果表明, 负载的银纳米粒子粒径为几十纳米至100 nm。而银纳米粒子的负载量可由聚丙烯酸的接枝率控制。细菌平板计数法测试结果表明, 所制备的杂化膜具有优异的抗菌性, 对大肠杆菌的抗菌率高达100%。

关键词: 膨化聚四氟乙烯薄膜, 辐射接枝, 聚丙烯酸, 纳米银, 抗菌性

动态加载过程中石英玻璃诱导水的快速结晶相变 113

李永宏^{a,b*}, 张宁超^b, 王文鹏^b, 刘福生^b (a. 运城学院物理与电子工程系, 运城 044000; b. 西南交通大学高压科学与技术实验室, 成都 610031)

摘要: 在气炮加载试验中利用弹载光源原位测试技术, 观测了夹于石英玻璃之间的水在动态压缩过程中的透光特性。通过其光透射特性研究了水的冲击相变。实验结果发现液态水在动态冲击压缩过程中, 其压力低于2 GPa就出现透明性变差的现象, 而且水的透明性下降与石英玻璃的存在有关, 是一种石英诱导水的结晶相变现象。

关键词: 水, 石英玻璃, 冲击, 相变

北京机动车限行期间苯和甲苯的DOAS测量 119

李素文^{a,b}, 谢品华^b, 韦民红^a, 王江涛^a (a. 淮北师范大学物理与电子信息学院, 淮北 235000; b. 中国科学院环境光学与技术重点实验室, 合肥 230031)

摘要: 基于差分光学吸收光谱(DOAS)技术在北京机动车限行期间8月7日到28日对苯和甲苯进行连续监测, 获取苯、甲苯的变化特征, 分析交通排放苯、甲苯和车流量关系。监测结果表明, 整个交通管制期间, 监测点苯与甲苯相关系数为0.8, 且二者比值为0.43~0.50, 充分证明苯系物具有同源性。限行时段苯的浓度下降11.4%, 甲苯下降12.8%, 而车流量下降11.8%, 因此苯和甲苯是北京机动车排放的主要来源。

关键词: DOAS, 苯和甲苯, 机动车限行, 交通排放, 车流量